Dyes and Pigments 173 (2020) 107851

Contents lists available at ScienceDirect

Dyes and Pigments

journal homepage: www.elsevier.com/locate/dyepig

Fluorescence and photoinduced proton transfer in the protolytic forms of fluorescein: Experimental and computational study

Marina A. Gerasimova[a,*], Felix N. Tomilin[a,b], Elena Yu. Malyar[a], Sergey A. Varganov[c], Dmitri G. Fedorov[d], Sergey G. Ovchinnikov[a,b], Evgenia A. Slyusareva[a]

[a] Siberian Federal University, Svobodny Prospect 79, Krasnoyarsk, 660041, Russia
[b] Kirensky Institute of Physics, Federal Research Center KSC SB RAS, Akademgorodok 50/38, Krasnoyarsk, 660036, Russia
[c] Department of Chemistry, University of Nevada, Reno, North Virginia Street 1664, Reno, NV, 89557-0216, United States
[d] Research Center for Computational Design of Advanced Functional Materials, National Institute of Advanced Industrial Science and Technology, Central 2, Umezono 1-1-1, Tsukuba, 305-8568, Japan

ARTICLE INFO

Keywords:
Fluorescein protolytic forms
Absorption
Fluorescence
TD-DFT
Proton transfer
Excited-state dissociation constant

ABSTRACT

In contrast to the well-studied absorption spectra of different protolytic forms of fluorescein, the complex structure of the fluorescence spectra in a wide pH range is not completely understood because of the interplay between emission and photoinduced proton transfer in the electronic excited states. We provide insight into this interplay through a combined analysis of the experimental data, obtained by absorption and steady-state fluorescence spectroscopy at pH 0.3–10.5, and the time-dependent density functional theory (TD-DFT). The TD-DFT based computational model is validated on dianion and used to model the spectra of other protolytic forms. The protolytic/tautomeric forms of fluorescein are classified according to the partial charges on the triple chromophore ring, and electronic transitions are analyzed in terms of changes in molecular geometries and orbitals. A linear regression analysis between the calculated and experimental results based on both absorption and well-understood dianionic and cationic fluorescence peaks is used to assign the monoanionic (496 nm), neutral quinoid (550 nm) and neutral zwitterionic (483 nm) fluorescence peaks, whose positions were not clear prior to this work. The values of the excited-state dissociation microconstants pk_a^* for different forms of fluorescein are calculated by means of the Förster cycle in conjunction with the spectroscopic measurements and computational data.

1. Introduction

Fluorescein and its derivatives are well-known fluorescent probes [1–4]. Owing to their high absorptivity, quantum yield and photostability, fluorescein-based dyes are used as fluorescent sensors for labeling and imaging of colorless systems (living cells [2–4], drug delivery systems [5], enzymes [6], proteins [7], micelles [8], carbon nanotubes [9]), FRET-based sensors [10,11], as well as spectral tracers for pH [2,4,6,9–13], viscosity [13] and pressure [14] changes in local environment. Due to changes in the chromophore structure upon protonation (Fig. 1), fluorescein can be used to study ionic bonding in proton donating biological macromolecules and polymers [15]. Except for extremely acidic or alkaline media, fluorescein (R) dissociation in aqueous solutions involves the following stages [16]:

$$H_3R^+ \xleftrightarrow{{}_pK_{a0} = 2.25} H_2R + H^+, \quad (1)$$

$$H_2R \xleftrightarrow{{}_pK_{a1} = 4.23} HR^- + H^+, \quad (2)$$

$$HR^- \xleftrightarrow{{}_pK_{a2} = 6.32} R^{2-} + H^+, \quad (3)$$

where $K_{a(1-z)}$ is the ground-state dissociation constant for the reaction $H_iR^z \leftrightarrow H_{i-1}R^{z-1} + H^+$. Thus, fluorescein in the ground state may exists as dianion (D), monoanionic species (carboxylate anion (MI) and phenolate anion (MII)), neutral species (lactone (L), quinoid (Q), zwitterion (Z)), and cation (C).

The absorption spectra of the protolytic forms of fluorescein in water have been studied in details using experimental [12,16–20] and theoretical [21–34] methods. These studies revealed the signatures of different protolytic/tautomeric forms in the absorption spectra [16,17,19]. Electronic structure calculations on fluorescein have been performed using semiempirical methods [21,22,30,34] and density functional theory (DFT) [21–29,31,32]. Different density functionals

* Corresponding author.
E-mail address: marina_2506@mail.ru (M.A. Gerasimova).

https://doi.org/10.1016/j.dyepig.2019.107851
Received 27 March 2019; Received in revised form 27 July 2019; Accepted 29 August 2019
Available online 30 August 2019

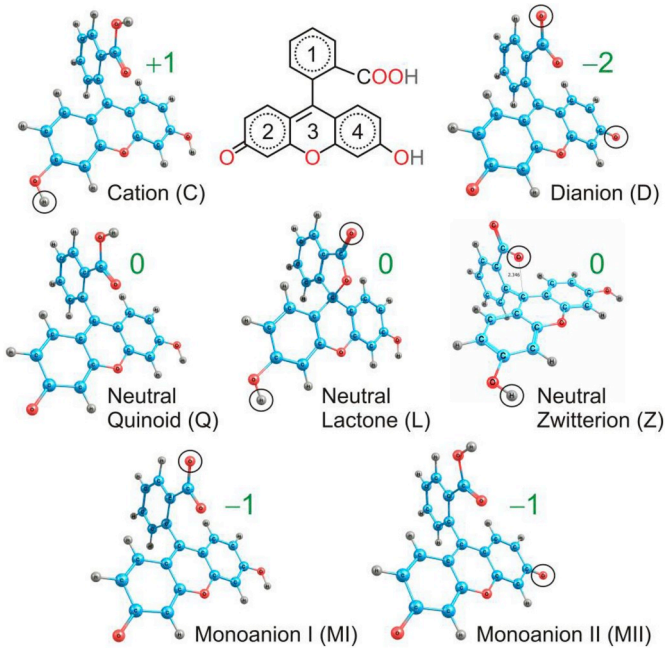

Fig. 1. Protolytic and tautomeric forms of fluorescein with the charges shown in green. The protons responsible for changes from the quinoid to other forms are highlighted by the circles. The carbon, oxygen and hydrogen atoms are blue, red and grey, respectively. (For interpretation of the references to color in this figure legend, the reader is referred to the Web version of this article.)

(B3PW91 [32], BP86 [29], PBE0 [24], CAM-B3LYP/RI-CC2 [25], B3LYP [21–23,25–29]), basis sets (6–31G(p,d) [29], 6–311G(p,d) [32], 6–311 + +G(p,d) [21,22], LANI2DZ [27]), and both implicit (COSMO [25] and PCM [22,25,27,29,31]) and explicit solvent [21,22,34] models have been used. These studies have been mostly focused on the dianionic form [21,22,24–27,29,30,32] and showed some deviations from the experimental results: for example, the first absorption peak of fluorescein dianion in water has been predicted to be at 412–485 nm, whereas the experimental absorption maximum is at 490 nm.

In contrast to the absorption spectra, computational studies of the fluorescein emission spectra are much scarcer. Most of the computational results were obtained for the dianionic form [25,26,29]. Moreover, in the previous experimental studies [12,16–18,35–38], there is no in-depth analysis of fluorescence peaks of protolytic/tautomeric forms, except for those that exist in a pure form (dianion, cation). Additionally, the experimental reports are often contradictory regarding the number of the fluorescent species. In some cases [17,39], only three fluorescent forms have been accounted for (dianion, monoanion and cation), whereas in others [16,18] the neutral form has also been considered. The interpretation of the experimental data is complicated by a possible proton transfer in the excited states (i.e., absorption and fluorescence can occur in different protolytic forms) [16–18,35,38,40]. This leads to large differences in the reported fluorescence quantum yields for the individual protolytic/tautomeric forms: 0; 0.39, 0.9–1 for cation, 0–0.3 for neutral species, and 0.26–0.37 for anion [16–18,35,36,38,39]. The photoinduced proton transfer has been observed in other pH-sensitive organic fluorophores, including coelenteramide and coelenteramide-containing photoproteins [41], as well as 1-hydroxypyrene-3,6,8-trisulfonate [42]. An additional difficulty in assigning spectral peaks arises from a wide overlap of vibronic fluorescence bands of the different protolytic and tautomeric forms coexisting in solution [16–19].

To the best of our knowledge, a comprehensive study of fluorescence spectra for all protolytic forms of fluorescein that coexist at different pH has not been reported before. The aim of this study is to clearly identify the fluorescein species (dianion, monoanion, neutral quinoid, neutral zwitterion and cation) in the fluorescence spectra in a wide pH range using combination of experimental and theoretical techniques.

2. Experimental and theoretical methods

2.1. Sample preparation and spectroscopic measurements

In this work, the sodium salt of fluorescein (C.I. 45350) was obtained from Fluka and used without additional purification. To prepare unbuffered aqueous solutions of fluorescein in the pH range of 0.3–10.5, distilled water, aqueous solutions of KOH, and hydrochloric acid were used. The dye concentration in solutions was 7 μM. Measurements were performed 30–40 min after preparation of solutions. The pH value of solutions was controlled with SevenCompact S220 pH/Ion meter (Mettler Toledo). The absorption spectra were recorded with a Lambda 35 spectrophotometer (PerkinElmer). The fluorescence spectra were measured on a Fluorolog 3–22 spectrofluorometer (Horiba Jobin Yvon). Fluorescein was excited at the wavelength of 420 nm. The obtained fluorescence spectra were corrected for the reabsorption, if necessary, and for sensitivity of the recording system. Standard quartz cells with cross sections of 10 × 10 mm were used to investigate solutions for L-geometry of excitation. All measurements were performed at room temperature.

2.2. Computational details

Two types of the time-dependent density functional theory with polarization continuum model (TD-DFT/PCM) calculations were carried out using the GAMESS suite of programs [43]. In the first type, denoted as PCM [44,45], electronic excitation energies and oscillator strengths were computed assuming solvent relaxation in the excited states (the same dielectric constant $\varepsilon = 78.39$ was used for the ground and excited states, NONEQ = .F. in GAMESS). In the second type [45], denoted as PCM*, non-equilibrium vertical excitation energies and oscillator strengths were calculated using the dielectric constant $\varepsilon_\infty = 1.776$ in TD-DFT by setting NONEQ = .T. in GAMESS. The geometry of the fluorescein dianion was fully optimized for the ground state with no symmetry constraints, separately in the gas phase and in solution. Then, the vertical excitation energies for absorption spectra were calculated as differences between the energies of the excited and ground states, both computed at the ground state geometries. The fluorescence energies were obtained as the vertical de-excitation energies corresponding to transitions between the excited and ground states, at the geometries of the excited states. To select an accurate level of theory for describing the absorption and fluorescence spectra the DFT calculations were carried out with the B3LYP, LC-BOP, and CAM-B3LYP functionals. The following basis sets were used: 6–31G(p,d), 6–311G(p,d) and 6–311 + +G(p,d) (Pople family); cc-pVDZ, and *aug*-cc-pVDZ (Dunning family). The results obtained using different solvent models and electronic structure levels of theory are reported in Tables S1–S2 in Supplementary materials.

The TD-DFT calculations of excitation energies were performed for the fluorescein forms with charges −2 (D form), −1 (MI, MII forms), 0 (L, Q, Z forms), and +1 (C form). The atomic coordinates for all forms are provided in Supplementary material. Two conformations corresponding to the different positions of hydrogen in the carboxyl group of MII, Q and C forms were investigated. The difference between the energies of two conformers of these protolytic/tautomeric forms was found to be about 1–7 kJ/mol. Fig. 1 shows the minimum energy structures of MII, Q, and C forms in which hydrogen of the carboxyl group is the furthest from the triple ring. To analyze the charge distribution in the different forms of fluorescein, the total charges on four rings (rings 1, 2, 3, and 4 in Fig. 1) were calculated (see Table S3 in Supplementary materials). The total ring charges were obtained by a summation of the Löwdin atomic charges on the carbon and oxygen atoms of the rings.

3. Results and discussion

3.1. Absorption and fluorescence spectra

Depending on pH, fluorescein in the ground state in aqueous solution can exist in four protolytic forms: dianion at 14 > pH > 4.0–4.5, monoanion at 8.5–9.0 > pH > 2.0–2.5, neutral species at 6.0–6.5 > pH > 0–0.5 and cation at 4.0–4.5 > pH > 0 (see Eqs. (1)–(3)) [16,17]. Only for two forms of fluorescein (dianion and cation) it is possible to detect the absorption spectrum of the individual form: under very alkaline and very acidic conditions. For the monoanionic and neutral species, one could choose the pH at which a desired form would prevail.

Based on the foregoing, we selected pH 10.5, 5.0, 3.0, 0.3, at which four protolytic forms of fluorescein in the ground state are dominant in aqueous solution [16–18]. At pH 10.5, fluorescein exists as the dianionic form. At pH 0.3, the fraction of the cationic form prevails (> 98–99%). At pH 5.0, fluorescein mainly exists in the monoanionic form (81–83%), and the rest fractions of the neutral (13–14%) and dianionic (3%) species are rather low. Finally at pH 3.0, the neutral form represents the major fraction (82–85%), while the monoanionic and cationic forms contribute 3–4%, and 11–14%, respectively.

The absorption spectra measured at the selected pH values are shown in Fig. 2. The presence of several maxima and shoulders in these spectra can be an evidence of (i) influence of vibrations, (ii) coexistence of several tautomeric forms with different characteristic maxima, and (iii) combination of transitions to higher electronic states. The following analysis is focused on the $S_0 \rightarrow S_1$ transition above 350 nm, where for the majority of ionic forms there is no contribution of the higher excited states transitions.

At pH 10.5 (Fig. 2a), fluorescein is in the dianionic D form with the absorption maximum at 490 nm. The short-wavelength shoulder near 465 nm has a vibrational nature. At pH 5.0 (Fig. 2b), the fluorescein spectrum has two prominent peaks (at 453 and 474 nm) and two shoulders (near 426 and 385 nm). Subtracting the small fractions of dianionic and neutral species, the spectrum of the individual monoanionic form is resolved with the main peak at 473 nm. The short-wavelength peak at 453 nm and the small shoulder near 426 nm are within several hundred wavenumbers of the main peak and attributed to the vibrational structure associated with the bonds stretching in the triple xanthene ring [46]. The shoulder near 385 nm lies significantly further from the main monoanion peak and could be due to transitions to a higher electronic state. At pH 3.0 (Fig. 2c), fluorescein characterized by the short-wavelength peak at 436 and the long-wavelength shoulder near 475 nm. It should be noted that although at pH 3.0 the fluorescein is predominantly in the neutral form, 70% of it belongs to the lactone colorless species [16], therefore the contribution of the cationic form to the absorption spectrum is more significant than it seemed initially. The decomposition of complex spectrum of fluorescein at pH 3.0 was performed (Fig. 2c) to obtain the spectrum of the individual tautomer and to associate the peak at 433 nm with the zwitterionic Z form and peak at 473 nm with the quinoid Q form. The spectrum of Q form is assumed to be identical to monoanionic MI form, while the spectrum of Z form is similar to the cationic one, but shifted to the blue region by 3 nm [16] or 4 nm in our study. The cationic form at pH 0.3 has the absorption maximum at 437 nm (Fig. 2d).

A mirror-like symmetry in the normalized [47] absorption and fluorescence spectra is found only at pH 10.5 (Fig. 2a, Fig. S1 in Supplementary material). At such high pH, fluorescein is in its dianionic form in both the ground and excited states, and having the mirror-symmetry suggests that the vibrational structures of electronic excited and ground states are similar. At pH 5.0, 3.0, and 0.3 there is no mirror symmetry between the absorption and fluorescence spectra (Fig. 2b–d, see Fig. S1 for other pH). This could be explained by the following factors: a) contributions to emission from several different forms (these contributions are determined not only by the concentrations but also by the molar extinction coefficients at the excitation wavelength and the quantum yield of each form), b) significant structural changes in the excited state and solvent reorganization, c) proton transfer in the excited states leading to the absorption and emission from different forms.

There is no consensus in the literature on the number of fluorescent forms of fluorescein. Sjöback et al. [17] and Leonhardt et al. [39] reported that only the cationic, monoanionic, and dianionic forms emit (the neutral form in the excited state undergoes a transformation to the monoanionic form). However, Klonis et al. [16] and Martin et al. [18] reported that the quinoid form is also fluorescent. As can be seen in

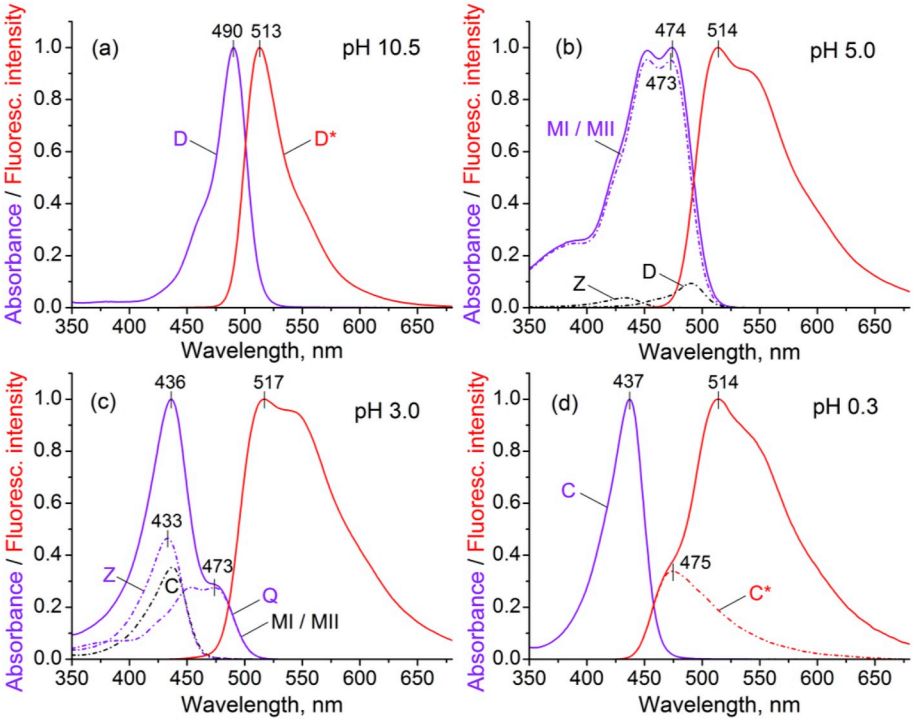

Fig. 2. Experimental absorption (violet) and fluorescence (red) spectra of fluorescein at (a) pH 10.5, (b) pH 5.0, (c) pH 3.0, and (d) pH 0.3. The decomposition of complex spectrum at pH 5.0, 3.0 and 0.3 into the individual protolytic/tautomeric forms is shown as dotted lines. The resolved spectrum of cation fluorescence was taken from Ref. 17, 18. (For interpretation of the references to color in this figure legend, the reader is referred to the Web version of this article.)

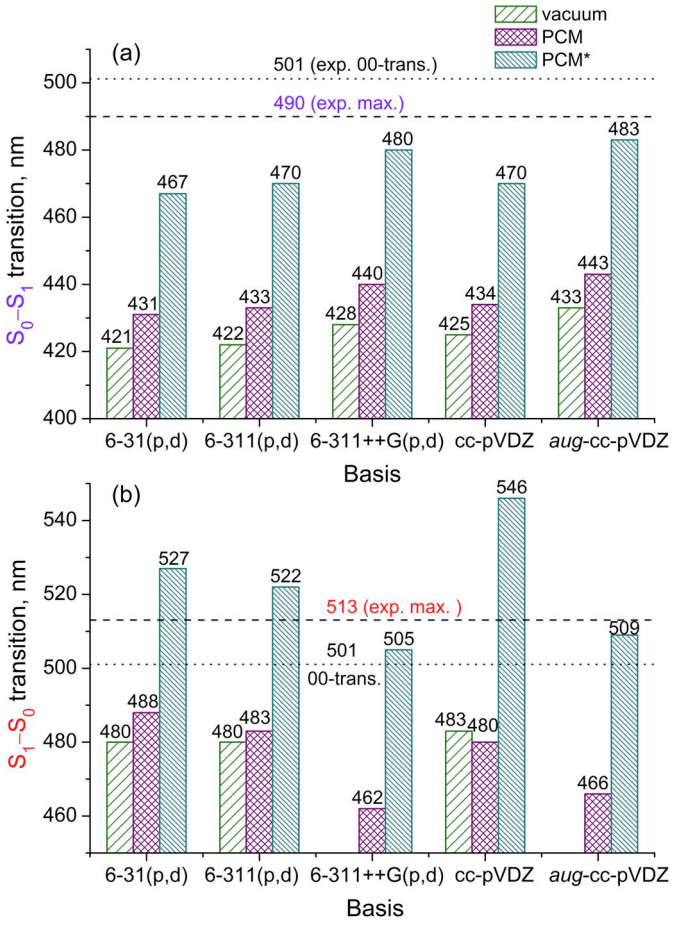

Fig. 3. $S_0 \rightarrow S_1$ (a) and $S_1 \rightarrow S_0$ (b) transition wavelengths of the fluorescein dianion calculated using the B3LYP functional, and different basis sets and solvation models. The experimental values corresponding to the maxima in absorption and fluorescence spectra (dashed lines) and 0-0 transition (dotted line) are shown.

Fig. 2a, the dianionic D* form, which dominates at pH 10.5, emits at 513 nm (symbol "*" next to the form label indicates an excited state). At pH 0.3, the evident shoulder near 470–480 nm belongs to C* form (Fig. 2d) [16–18,37,48]. At very acidic conditions (5–10 M H_2SO_4 or HCl), this shoulder becomes a dominant peak at 475 nm (see dotted line in Fig. 2d). The fluorescence maxima in the range of $0.3 < pH < 5.0$ lie around 514–517 nm (Fig. 2b–d); and the spectra are significantly broadened relative to the dianion spectrum. For instance, at pH 5.0, the broadening near 480–500 nm and the shoulder near 550 nm, which gradually vanishes as pH decreases, are observed. These observations indicate that at the intermediate pH the fluorescence spectrum contains the contributions from several protolytic forms.

3.2. Method validation for modeling the spectra

In general, theoretical 0-0 transition wavelengths should be compared with the crossing points between absorption and fluorescence spectra. However, since the experimental wavelengths of the 0-0 transitions and the peak maxima differ by only about 10 nm (Fig. 3), we compare theoretical vertical transitions with the peak maxima. As the quality of the basis set within the Pople and Dunning families is improved, the predicted wavelength of the $S_0 \rightarrow S_1$ transition increases and approaches the experimental maxima, for both the gas phase (vacuum) and especially the solvent (PCM and PCM*) calculations (Fig. 3). These results also show the importance of including diffuse functions to accurately describe the anionic forms. For fluorescein dianion, changing the basis set from 6–311G(p,d) to 6–311 + + G(p,d) and from cc-pVDZ to *aug*-cc-pVDZ results in 6–10 nm and 7–13 nm wavelength shifts, respectively (Fig. 3a). In contrast, increasing the size of the basis set from double- to triple-zeta has small effect on the transition wavelengths, as seen from comparing the 6–31G(p,d) and 6–311G(p,d) results. To test the basis set convergence, the TD-DFT energy calculations were performed at the B3LYP/PCM*/*aug*-cc-pVTZ level of theory using the B3LYP/PCM*/*aug*-cc-pVDZ optimized geometry. This increase in basis set resulted in a less than 2 nm change in the transition wavelength. The fluorescence wavelengths are also accurately reproduced with *aug*-cc-pVDZ basis set (Fig. 3b).

The long-range corrected (LC) functionals, such as LC-BOP [49] and CAM-B3LYP [50], are often used for calculating the charge transfer transitions. However, we found that these functionals overestimate the transition wavelengths of fluorescein dianion compared to B3LYP (see Fig. S2 in Supplementary material). A similar conclusion has been reached by Zhou et al. [25], who used the CAM-B3LYP functional and obtained a value of 439 nm (2.83 eV) for the $S_0 \rightarrow S_1$ transition, which is 0.31 eV above the experimental value. For all electronic transitions calculated in this work, the measures of the spatial overlap between the occupied and virtual orbitals contributing to the electronic excitations, known as Λ-values [51], lie within $0.45 \leq \Lambda \leq 0.89$, which suggests the lack of a Rydberg character and a considerable localization of excitations within the chromophore. These findings are in agreement with Zhang et al. [52], who experimentally demonstrated that the photo-induced charge transfer in fluorescein is the least important among all xanthene dyes.

The transition wavelengths obtained with the non-equilibrium solvation model (PCM*) are in a better agreement with the experimental values than the equilibrium PCM wavelengths suggesting what the solvent relaxation time is shorter than the excited state lifetime [45]. Based on these preliminary calculations, the B3LYP/*aug*-cc-pVDZ/PCM* level of theory was selected and used in all calculations described below. For the dianionic form, this level of theory reproduces the experimental absorption and fluorescence wavelengths with a reasonable accuracy of 7 and 4 nm, respectively.

3.3. Identification of the fluorescein forms in the spectra

The results of TD-DFT for different forms of fluorescein are listed in Supplementary materials. Here, we focus on $S_0 \rightarrow S_1$ and $S_1 \rightarrow S_0$ transitions with the oscillator strength $f > 0.05$ and $0.45 \leq \Lambda \leq 0.89$ (see details in Table S4). In Table 1, the TD-DFT results are compared with the maxima of the absorption and fluorescence spectra for the different protolytic forms of fluorescein.

For the absorption spectra, the computational results are consistent with experimental values. There are no experimental values for the lactonic form, which absorbs in the UV range, and two sets of theoretical values for the MI and MII tautomers of monoanion. For the fluorescence spectra, an unambiguous correspondence between the experimental and theoretical results can be established only for the dianionic and cationic forms.

All protolytic/tautomeric forms of fluorescein can be classified according to the charge of the triple ring (rings 2, 3 and 4 in Fig. 1) in the ground electronic state (Table 1 and Table S3). D and MII forms with large negative charges on the triple ring (−1.16 and −1.07) are assigned to group 1, while MI and Q forms with smaller negative charges (−0.21 and −0.11) are assigned to group 2. Group 3 includes Z and C forms with large positive charges (0.61 and 0.89). The colorless lactonic L form is characterized by a nearly zero charge and distinct from other protolytic forms. The observed similarities in the absorption spectra of MI and Q forms (group 2), as well as C and Z forms (group 3) correlate with the similar charges on the triple ring (Table 1). Similar charges of the triple ring in D and MII forms (group 1) correlate with the fact that the calculated absorption wavelengths for these forms are close (483 and 495 nm). The absorption wavelengths of Z and C forms are also

Table 1
Properties of protolytic and tautomeric forms of fluorescein in the ground and excited states.

Form	Charge	Group (charge)[a]	Absorption				Fluorescence		
			Theory[b]		Exp.[c]		Theory[b]		Exp.[c]
			λ_{abs}, nm	f_{abs}	λ_{abs_max}, nm	ε_{max}, 10^4 mol l^{-1} cm^{-1}	λ_{fl}, nm	f_{fl}	λ_{fl_max}, nm
D	–2	1 (–1.16)	483	1.16	490	8.0	509	1.05	513
MI	–1	2 (–0.21)	448	0.84	473	2.9	483	0.69	?[d]
MII	–1	1 (–1.07)	495	1.11	473	2.9	626	0.35	–
L	0	4 (0.07)	277	0.09	–	–	284	0.14	–
Z	0	3 (0.61)	412	0.18	433	1.3	467	0.06	?[d]
Q	0	2 (–0.11)	452	0.87	473	0.4	555	0.57	?[d]
C	+1	3 (0.89)	412	0.91	437	5.3	453	0.14	475[e]

[a] Protolytic forms are grouped according to the triple ring Löwdin charge (see Table S3 in Supplementary material) in the ground electronic state.
[b] B3LYP/*aug*-cc-pVDZ/PCM*, λ_{abs} and f_{abs} are the absorption (abs) wavelength and oscillator strength of $S_0 \rightarrow S_1$ transition, respectively; λ_{fl} and f_{fl} are the fluorescence (fl) wavelength and oscillator strength of $S_1 \rightarrow S_0$ transition, respectively.
[c] Measured in this work: λ_{abs_max} and λ_{fl_max} are the maximum wavelengths in the absorption and fluorescence spectra, respectively; ε_{max} is the molar extinction coefficient at λ_{abs_max}.
[d] Values of λ_{fl_max} for the monoanionic, quinoid, and zwitterionic forms labeled with "?" cannot be determined unambiguously.
[e] The average value of cation maximum is taken from Ref. [17, 18, 37, 47].

similar (412 and 412 nm according to theory, 433 and 437 nm according to experiment). The same is true for MI and Q forms with the experimental absorption wavelengths of 473 and 473 nm, respectively, and the theoretical values of 448 and 452 nm. An important aspect of the grouping is that the triple ring chromophore has the same chemical composition in each group, whereas between the groups, the chromophore can differ by 1–3 protons.

Molecular orbitals involved in the $S_0 \rightarrow S_1$ transitions are shown in Fig. 4. D and MII forms (group 1) have similar occupied and virtual orbitals localized on the triple chromophore ring. The same is true for MI and Q forms (group 2), as well as for C form (group 3). The localization of the orbitals, involved in the excitation, on the chromophore leads to large values of oscillator strength (from 0.84 to 1.16) for these forms. In contrast, in Z form (group 3), only the virtual orbital is centered on the chromophore, while the occupied orbital is located mostly on ring 1, producing the much smaller oscillator strength f_{abs} of 0.18. Finally, the occupied and virtual orbitals of L form (group 4) are completely localized on the chromophore and ring 1, respectively. Such localization produces very small oscillator strength f_{abs} of 0.09. There is a correlation between the oscillator strengths and the experimental extinction coefficients, except for the quinoid Q form (Table 1).

Electronic excitation leads to the distortion of the ground state geometry mainly affecting several dihedral angles in all protolytic/tautomeric forms (see details in Table S5). In the excited state, Q and MII forms are the most distorted, which explains their larger Stokes shifts (103 and 131 nm) compared to other forms (26–55 nm), as can be seen from the calculated wavelengths in Table 1. A significant Stokes shift in Q form agrees with the earlier predictions from the LR-PCM/TD-B3LYP calculations (130 nm) [25]. Excited state molecular orbitals involved in the $S_1 \rightarrow S_0$ transition are shown in Fig. S3 in Supplementary materials.

The linear regression plot in Fig. 5 shows that there is a strong correlation with coefficient $R = 0.987$ between the previously assigned experimental and calculated wavelengths for the absorption (D, MI, Q, Z and C forms) as well as for fluorescence (D* and C* forms) transitions. This dependence plotted in transition energies provides the same fitted parameters with $R = 0.988$. The high correlation justifies the use of the linear regression to identify the signatures of other protolytic forms in the absorption and fluorescence spectra of fluorescein.

First, the linear regression can be used to clarify the assignment of tautomeric forms in the experimental spectra. It was argued earlier [16,19] that MI form with absorption at 473 nm, rather than MII form, is dominant in solution at equilibrium according to Eq. (2). As can be seen in Fig. 5, the MI point lies on the regression line – a strong indication that MI form is present in solution, whereas the MII point (empty violet circle) falls out from the regression. Second, the fluorescence wavelengths for the neutral quinoid Q*, monoanionic MI*, and neutral zwitterionic Z* forms, denoted by "?" in Table 1, now can be identified as 550, 496, and 483 nm, respectively. Indeed, the 550 and 496 nm bands can be seen as the shoulder and broadening of spectrum near the main fluorescence peak (Fig. 6a). A possible weak fluorescence of the zwitterion at 483 nm can be explained by the small value of the predicted oscillator strength ($f_{fl} = 0.06$ in Table 1). Martin et al. [18] and Klonis et al. [16] suggested that the zwitterion fluorescence cannot be observed at all because in the excited state this form is quickly transforms to the cationic and/or monoanionic forms.

The relative change in the emission intensity at 475, 496 and 550 nm as a function of pH is shown in Fig. 6b. The intensities at these wavelengths (associated with C*, MI* and Q* forms) behave differently, indicating that the changes indeed come from different forms of fluorescein. At the same time, there is no strong correlation of these intensity ratios with the concentrations of the corresponding protolytic/tautomeric species in the ground state (see bottom of Fig. 6b). This fact may indicate a photoinduced proton transfer in the excited states of different protolytic forms.

Summarizing, in the range of $0.3 < pH < 7.0$, the complex shape of the fluorescence spectra can be interpreted as a result of fluorescence of different protolytic and tautomeric species of fluorescein. In particular, the broadening near 480–500 nm is attributed to the presence of the monoanionic MI* form. The peak at 550 nm is attributed to the quinoid Q* form, and the shoulder near 475 nm at low pH values ($pH < 0.3$–1.0) corresponds to the cationic C* form. The predominant fluorescent form in a wide pH range is the dianionic D* form with fluorescence at 513 nm. To a great extent this form determines the position of fluorescence maximum of the protolytic and tautomeric forms mixture due to the dianionic form's highest quantum yield among the fluorescein species [16] and possible multistep proton transfer.

3.4. Determination of the excited-state microconstants

In order to distinguish ionic equilibriums for various tautomeric forms, we evaluate the dissociation microconstants, denoted as pk_a for the ground state and pk_a^* for excited states. It is well-known that an excitation and external proton concentration have a strong effect on the dissociation constant and photoinduced proton transfer [42,53]. To the best of our knowledge, the values of pk_a^* for the whole set of fluorescein protolytic/tautomeric forms have not been reported. The experimental determination of these values is complicated by the fact that the

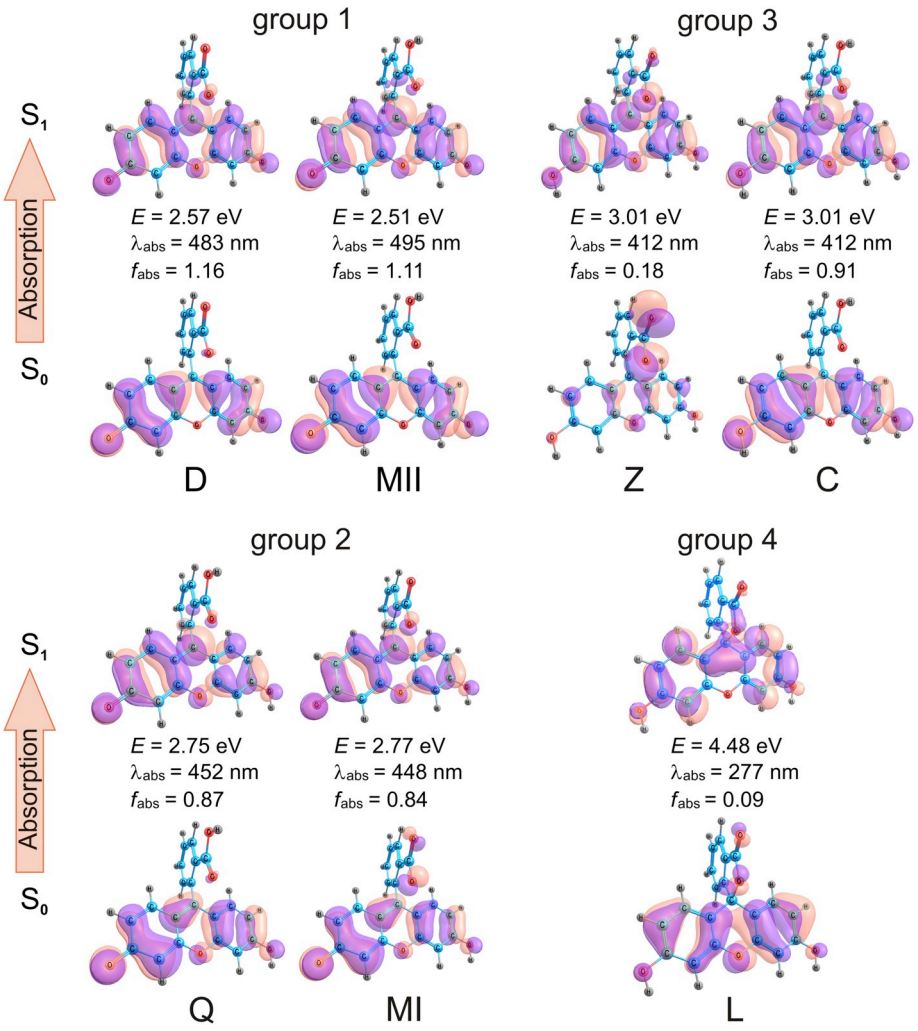

Fig. 4. Pairs of the occupied and virtual molecular orbitals involved in $S_0 \rightarrow S_1$ excitations at the ground state geometries. Excitation energies (E), corresponding absorption wavelengths (λ_{abs}), and oscillator strengths (f_{abs}) are shown.

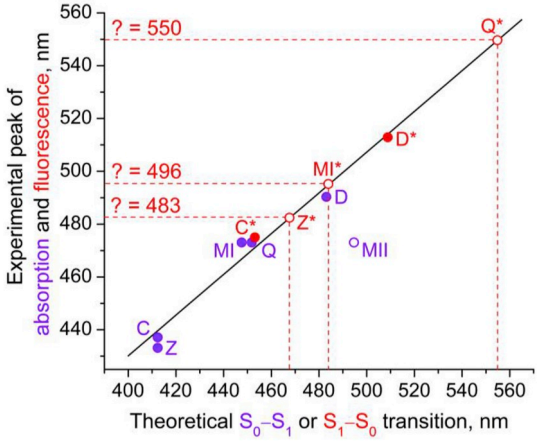

Fig. 5. Correlation between the calculated and experimental wavelengths in the absorption (filled violet circles) and fluorescence (filled red circles) spectra of different protolytic and tautomeric forms of fluorescein. Empty red circles show theoretical predictions for the cases where experimental values are not available (fluorescence of MI*, Q* and Z* forms). (For interpretation of the references to color in this figure legend, the reader is referred to the Web version of this article.)

equilibrium could not be established during the short lifetime of the excited state [54]. In the case of reaching the equilibrium a method for estimating pk_a^* based on the Förster cycle (Fig. 7a) could be used [42,53]. This method requires only the values of the energy gaps between the corresponding ground and excited states of HR and R^- forms:

$$\Delta pk_a = pk_a - pk_a^* = hc\frac{\tilde{\nu}_{0-0}^{HR} - \tilde{\nu}_{0-0}^{R^-}}{2.3kT}, \quad (4)$$

where h is the Plank constant, c is the speed of light, k is the Boltzmann constant, T is the temperature. The wavenumber $\tilde{\nu}_{0-0}$ corresponding to the 0-0 electronic transition can be estimated by averaging the positions of the absorption ($\tilde{\nu}_{abs} = 1/\lambda_{abs\_max}$) and fluorescence ($\tilde{\nu}_{fl} = 1/\lambda_{fl\_max}$) maxima:

$$\tilde{\nu}_{0-0} = \frac{\tilde{\nu}_{abs} + \tilde{\nu}_{fl}}{2} \quad (5)$$

The wavelengths from Table 1 and Fig. 5 were used in Eq. (5) to estimate the 0-0 transitions of the fluorescein protolytic/tautomeric forms listed in Fig. 7a. The excited-state pk_a^* values (Fig. 7b, top scheme) were calculated using the ground-state microconstants (Fig. 7b, bottom scheme) [16]. The calculated pk_a^* values differ significantly from the corresponding ground-state values of pk_a, which implies the change in equilibrium of fluorescein species in the excited state compared to the ground state. The difference between the ground-state and excited-state microconstants is considerable and reaches 4.8 for cationic − quinoid equilibrium. For this case the pk_a^* of −1.6 is

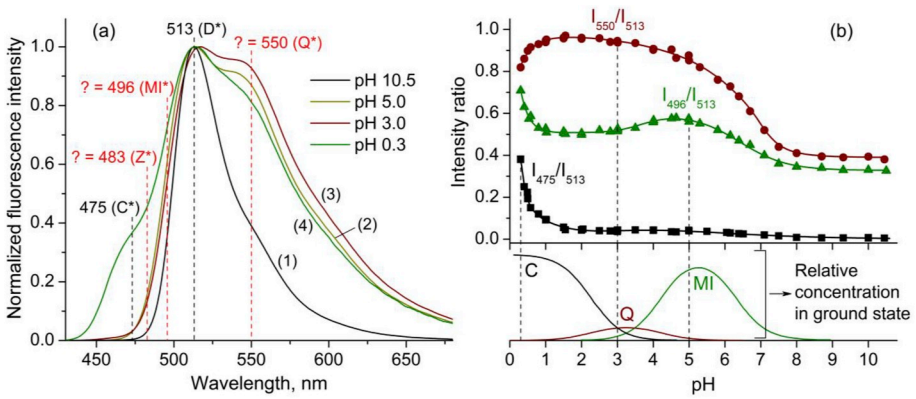

Fig. 6. (a) Experimental fluorescence spectra of fluorescein at (1) pH 10.5, (2) pH 5.0, (3) pH 3.0, and (4) pH 0.3. The peaks for MI*, Z*, and Q* forms are assigned using the linear regression shown in Fig. 5. (b) pH dependence of the intensity ratios at wavelengths of 475–513 nm (black squares), 496–513 nm (green triangles), and 550 to 513 nm (brown cycles). The relative concentrations of cationic C, neutral quinoid Q and monoanionic MI forms in the ground state are shown at the bottom, the data are taken from ref. 16. (For interpretation of the references to color in this figure legend, the reader is referred to the Web version of this article.)

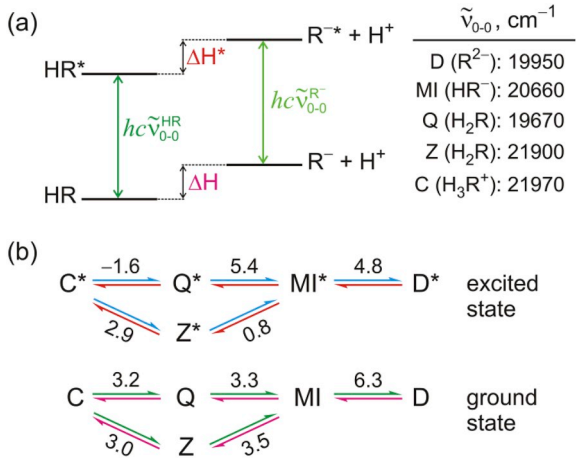

Fig. 7. (a) Electronic energy levels of the acid (HR) and conjugated base (R^-) forms of fluorescein in the ground and excited states (Förster cycle), and changes of the ground state (ΔH) and excited state (ΔH*) enthalpies. (b) Transitions between various forms of fluorescein in the excited and ground states. The values of the excited state microconstant pk_a^* obtained from Eq. (4), and the ground state microconstant pk_a taken from ref. 16 are shown.

comparable with the excited-state dissociation constant for cationic − neutral equilibrium obtained by Förster cycle [37] for fluorescein (−1.3) and by time-resolved fluorescent spectroscopy [55] for difluorofluorescein (−1.8). The microconstant for dianionic − monoanionic equilibrium in excited state (6.0–6.3) reported previously [17,35] differs from the value obtained in the present study (4.8), however it remains smaller than the ground state pk_a.

We also calculated the pk_a^* values using an alternative (theoretical) method that relies on the Born–Haber thermodynamic cycle [56] to obtain the ground state pk_a and the TD-DFT excitation energies from Table 1 and Fig. 5 to obtain $\tilde{\nu}_{0-0}$ based on Eq. (5). This theoretical method predicts the pk_a^* values that are similar to ones obtained using the experimental absorption and fluorescence energies (see Table S6 for details).

The accuracy of the Förster cycle method is very sensitive to the 0-0 transition energy. In the case of Q* form, which has a considerable Stokes shift, the wavelength of 0-0 transition is hard to determine accurately, both from experimental spectra and electronic structure calculations. A more accurate determination of the 0-0 transition energies requires detailed information on the vibrational structure of the absorption and fluorescence spectra [53]. Nevertheless, the predicted pk_a^* values are consistent with the experimental data (Fig. 6) revealing a significant contribution of the Q* form to the fluorescence spectra of fluorescein at pH 0.3–5.0. The computational part of this work can be extended to nonadiabatic molecular dynamics simulations [57,58] to study the excited state proton transfer in detail. Such study is expected to provide a time-resolved picture of the interplay between photoinduced proton transfer and emission in different protolytic forms of fluorescein and similar compounds.

4. Conclusions

The interplay between fluorescence and photoinduced proton transfer in fluorescein has been investigated by analyzing its absorption and fluorescence spectra in the wide pH range of 0.3–10.5. The computational procedure based on the time-dependent density functional theory, including selection of density functional, basis set, and specific form of the polarizable continuum model, has been validated on the dianionic form of fluorescein for which the experimental absorption and fluorescence wavelengths are known. The application of this computational procedure to other protolytic forms (dianion, monoanion, neutral quinoid, neutral zwitterion, neutral lactone and cation) has revealed the principal role of the partial charge on triple chromophore ring in determining the absorption wavelengths. The electronic transitions have been analyzed in terms of molecular geometry and orbital changes in ground and excited states.

The signatures of the fluorescein monoanionic MI* (496 nm), neutral quinoid Q* (550 nm), and possibly neutral zwitterionic Z* (483 nm) forms in multicomponent fluorescence spectra have been identified based on the linear regression between the calculated and experimentally known wavelengths. The excited-state dissociation microconstants pk_a^* for the set of protolytic/tautomeric fluorescein forms have been estimated by means of the Förster cycle method using the spectroscopic measurements and computational data.

The obtained results will be useful for accurate measurements of fluorescence quantum yield of protolytic forms, as well as for elucidation of the excited states kinetics involving both fluorescence and photoinduced proton transfer. The proposed approach, based on experimental and computational spectroscopic methods, can be applied to other organic fluorescent labels (e.g., fluorescein derivatives and coelenteramide-containing photoproteins), in which the direct identification of protolytic/tautomeric forms in experimental fluorescence spectra is hindered by the complex multistep proton transfer in the excited states.

Acknowledgments

This work is supported by the Russian Foundation for Basic Research, Russia (project 19-02-00450). S.A.V. thanks the National Science Foundation, United States for financial support through a CAREER Award (CHE-1654547).

Appendix A. Supplementary data

Supplementary data to this article can be found online at https://doi.org/10.1016/j.dyepig.2019.107851.

References

[1] Zheng H, Zhan XQ, Bian QN, Zhang XJ. Advances in modifying fluorescein and rhodamine fluorophores as fluorescent chemosensors. Chem Commun 2013;49:429–47https://doi.org/10.1039/c2cc35997a.

[2] Urano Y, Kamiya M, Kanda K, Ueno T, Hirose K, Nagano T. Evolution of fluorescein as a platform for finely tunable fluorescence probes. J Am Chem Soc 2005;127:4888–94https://doi.org/10.1021/ja043919h.

[3] Xiong X, Song F, Chen G, Sun W, Wang J, Gao P, et al. Construction of long-wavelength fluorescein analogues and their application as fluorescent probes. Chem Eur J 2013;19:6538–45https://doi.org/10.1002/chem.201300418.

[4] Li G, Zhang B, Song X, Xia Y, Yu H, Zhang X, et al. Ratiometric imaging of mitochondrial pH in living cells with a colorimetric fluorescent probe based on fluorescein derivative. Sens Actuators, B 2017;253:58–68https://doi.org/10.1016/j.snb.2017.06.065.

[5] Bazylevich A, Patsenker LD, Gellerman G. Exploiting fluorescein based drug conjugates for fluorescent monitoring in drug delivery. Dyes Pigm 2017;139:460–72https://doi.org/10.1016/j.dyepig.2016.11.057.

[6] Wolf A, Schneider C, Kim TY, Kirchberg K, Volz P, Alexiev U. A simulation-guided fluorescence correlation spectroscopy tool to investigate the protonation dynamics of cytochrome *c* oxidase. Phys Chem Chem Phys 2016;18:12877–85https://doi.org/10.1039/c5cp07925j.

[7] Abou-Zied OK, Sulaiman SAJ. Site-specific recognition of fluorescein by human serum albumin: a steady-state and time-resolved spectroscopic study. Dyes Pigm 2014;110:89–96https://doi.org/10.1016/j.dyepig.2014.05.005.

[8] Dutt GB. Do ionic and hydrophobic probes sense similar microenvironment in Triton X-100 nonionic reverse micelles? J Chem Phys 2008;129:014501https://doi.org/10.1063/1.2946705.

[9] Ghini G, Trono C, Giannetti A, Puleo GL, Luconi L, Amadou J, et al. Carbon nanotubes modified with fluorescein derivatives for pH nanosensing. Sens Actuators, B 2013;179:163–9https://doi.org/10.1016/j.snb.2012.10.022.

[10] Saha J, Roy AD, Dey D, Bhattacharjee D, Paul PK, Das R, et al. Effect of zinc oxide nanoparticle on fluorescence resonance energy transfer between fluorescein and rhodamine 6G. Spectrochim Acta A 2017;175:110–6https://doi.org/10.1016/j.saa.2016.12.002.

[11] Chen J, Tang Y, Wang H, Zhang P, Li Y, Jiang J. Design and fabrication of fluorescence resonance energy transfer-mediated fluorescent polymer nanoparticles for ratiometric sensing of lysosomal pH. J Colloid Interface Sci 2016;484:298–307https://doi.org/10.1016/j.jcis.2016.09.009.

[12] Slyusareva EA, Gerasimova MA. pH-Dependence of the absorption and fluorescent properties of fluorone dyes in aqueous solutions. Russ Phys J 2014;56:1370–7https://doi.org/10.1007/s11182-014-0188-8.

[13] Patil VS, Padalkar VS, Tathe AB, Sekar N. ESIPT-inspired benzothiazole fluorescein: photophysics of microenvironment pH and viscosity. Dyes Pigm 2013;98:507–17https://doi.org/10.1016/j.dyepig.2013.03.019.

[14] Johann RM. Indicating pressure and environmental effects by means of the spectral shift with rhodamine B and fluorescein. AIP Adv 2015;5:77175https://doi.org/10.1063/1.4927687.

[15] Slyusareva EA, Gerasimova MA, Sizykh AG, Gornostaev LM. Spectral and fluorescent indication of the acid-base properties of biopolymer solutions. Russ Phys J 2011;54:485–92https://doi.org/10.1007/s11182-011-9643-y.

[16] Klonis N, Sawyer WH. Spectral properties of the prototropic forms of fluorescein in aqueous solution. J Fluoresc 1996;6:147–57https://doi.org/10.1007/BF00732054.

[17] Sjöback R, Nygren J, Kubista M. Absorption and fluorescence properties of fluorescein. Spectrochim Acta A 1995;51. L7–21 https://doi.org/10.1016/0584-8539(95)01421-P.

[18] Martin MM, Lindqvist L. The pH dependence of fluorescein fluorescence. J Lumin 1975;10:381–90https://doi.org/10.1016/0022-2313(75)90003-4.

[19] Mchedlov-Petrossyan NO, Kukhtik VI, Alekseeva VI. Ionization and tautomerism of fluorescein, rhodamine B, N,N-diethylrhodol and related dyes in mixed and non-aqueous solvents. Dyes Pigm 1994;24:11–35https://doi.org/10.1016/0143-7208(94)87009-8.

[20] Diehl H, Horchak-Morris N. Studies on fluorescein – V. The absorbance of fluorescein in the ultraviolet, as a function of pH. Talanta 1987;34:739–41https://doi.org/10.1016/0039-9140(87)80232-1.

[21] Silva DL, Barreto RC, Lacerda Jr. EG, Coutinho K, Canuto S. One- and two-photon absorption of fluorescein dianion in water: a study using S-QM/MM methodology and ZINDO method. Spectrochim Acta A 2014;119:63–75https://doi.org/10.1016/j.saa.2013.04.035.

[22] Silva DL, Coutinho K, Canuto S. Electronic spectroscopy of biomolecules in solution: fluorescein dianion in water. Mol Phys 2010;108:3125–30https://doi.org/10.1080/00268976.2010.497779.

[23] Lebed AV, Biryukov AV, McHedlov-Petrossyan NO. A quantum-chemical study of tautomeric equilibria of fluorescein dyes in DMSO. Chem Heterocycl Comp 2014;50:336–48https://doi.org/10.1007/s10593-014-1481-8.

[24] Buonocore F, di Matteo A. New insights into oxidation properties and band structure of fluorescein dyes from ab initio calculations. Theor Chem Acc 2012;131:1130https://doi.org/10.1007/s00214-012-1130-1.

[25] Zhou P, Liu J, Yang S, Chen J, Han K, He G. The invalidity of the photo-induced electron transfer mechanism for fluorescein derivatives. Phys Chem Chem Phys 2012;14:15191–8https://doi.org/10.1039/c2cp42167d.

[26] Slyusareva EA, Tomilin FN, Sizykh AG, Tankevich EY, Kuzubov AA, Ovchinnikov SG. The effect of halogen substitution on the structure and electronic spectra of fluorone dyes. Opt Spectrosc 2012;112:671–8https://doi.org/10.1134/s0030400x12040194.

[27] Batistela VR, da Costa Cedran J, Moisés de Oliveira HP, Scarminio IS, Ueno LT, Eduardo da Hora Machado A, et al. Protolytic fluorescein species evaluated using chemometry and DFT studies. Dyes Pigm 2010;86:15–24https://doi.org/10.1016/j.dyepig.2009.11.002.

[28] Fazzi D, Castiglioni C, Negri F. Resistive memories based on Rose Bengal and related xanthene derivatives: insights from modeling charge transport properties. Phys Chem Chem Phys 2010;12:1600–9https://doi.org/10.1039/b920792a.

[29] Spagnuolo CC, Massad W, Miskoski S, Menendez GO, García NA, Jares-Erijman EA. Photostability and spectral properties of fluorinated fluoresceins and their biarsenical derivatives: a combined experimental and theoretical study. Photochem Photobiol 2009;85:1082–8https://doi.org/10.1111/j.1751-1097.2009.00565.x.

[30] Mchedlov-Petrossyan NO, Ivanov VV. Effect of the solvent on the absorption spectra and protonation of fluorescein dye anions. Russ J Phys Chem 2007;81:112–5https://doi.org/10.1134/s0036024407010219.

[31] Król M, Wrona M, Page CS, Bates PA. Macroscopic pK_a calculations for fluorescein and its derivatives. J Chem Theory Comput 2006;2:1520–9https://doi.org/10.1021/ct600235y.

[32] Tamulis A, Tamuliene J, Balevicius ML, Rinkevicius Z, Tamulis V. Quantum mechanical studies of intensity in electronic spectra of fluorescein dianion and monoanion forms. Struct Chem 2003;14:643–8https://doi.org/10.1023/B:STUC.0000007575.53499.d0.

[33] Jang YH, Hwang S, Chung DS. Tautomeric equilibrium of fluorescein in solution: ab initio calculations. Chem Lett 2001;30:1316–7https://doi.org/10.1246/cl.2001.1316.

[34] Fabian WMF, Schuppler S, Wolfbeis OS. Effects of annulation on absorption and fluorescence characteristics of fluorescein derivatives: a computational study. J Chem Soc, Perkin Trans 1996;2(0):853–6https://doi.org/10.1039/p29960000853.

[35] Yguerabide J, Talavera E, Alvarez JM, Quintero B. Steady-state fluorescence method for evaluating excited state proton reactions: application to fluorescein. Photochem Photobiol 1994;60:435–41https://doi.org/10.1111/j.1751-1097.1994.tb05130.x.

[36] Diehl H, Markuszewski R. Studies on fluorescein – VII. The fluorescence of fluorescein as a function of pH. Talanta 1989;36:416–8https://doi.org/10.1016/0039-9140(89)80213-9.

[37] Shah J, Pant DD. Kinetic study of excited state protolytic reaction in fluorescein cation. Curr Sci 1985;54:1040–3http://www.jstor.org/stable/24088578.

[38] Togashi DM, Szczupak B, Ryder AG, Calvet A, O'Loughlin M. Investigating tryptophan quenching of fluorescein fluorescence under protolytic equilibrium. J Phys Chem A 2009;113:2757–67https://doi.org/10.1021/jp808121y.

[39] Leonhardt H, Gordon L, Livingston R. Acid-base equilibriums of fluorescein and 2',7'-dichlorofluorescein in their ground and fluorescent states. J Phys Chem 1971;75:245–9https://doi.org/10.1021/j100672a011.

[40] Mezer A, Friedman R, Noivirt O, Nachliel E, Gutman M. The mechanism of proton transfer between adjacent sites exposed to water. J Phys Chem B 2005;109:11379–88https://doi.org/10.1021/jp046213i.

[41] Shimomura O, Teranishi K. Light-emitters involved in the luminescence of coelenterazine. Luminescence 2000;15:51–8https://doi.org/10.1002/(SICI)1522-7243(200001/02)15:1%3C51::AID-BIO555%3E3.0.CO;2-J.

[42] Lakowicz JR. Principles of fluorescence spectroscopy. third ed. New York: Springer Science+Business Media; 2006https://doi.org/10.1007/978-0-387-46312-4.

[43] Schmidt MW, Baldridge KK, Boatz JA, Elbert ST, Gordon MS, Jensen JH, et al. General atomic and molecular electronic structure system. J Comput Chem 1993;14:1347–63https://doi.org/10.1002/jcc.540141112.

[44] Tomasi J, Mennucci B, Cammi R. Quantum mechanical continuum solvation models. Chem Rev 2005;105:2999–3094https://doi.org/10.1021/cr9904009.

[45] Cossi M, Barone V. Time-dependent density functional theory for molecules in liquid solutions. J Chem Phys 2001;115:4708–17https://doi.org/10.1063/1.1394921.

[46] Wang L, Roitberg A, Meuse C, Gaigalas AK. Raman and FTIR spectroscopies of fluorescein in solutions. Spectrochim Acta A 2001;57:1781–91https://doi.org/10.1016/S1386-1425(01)00408-5.

[47] Birks JB, Dyson DJ. The relations between the fluorescence and absorption properties of organic molecules. Proc R Soc Lond A 1963;275:135–48https://doi.org/10.1098/rspa.1963.0159.

[48] Ali M, Kumar V, Pandey S. Unusual fluorescein prototropism within aqueous acidic 1-butyl-3-methylimidazolium tetrafluoroborate solution. Chem Commun 2010;46:5112–4https://doi.org/10.1039/c0cc00620c.

[49] Tsuneda T, Suzumura T, Hirao K. A new one-parameter progressive Colle–Salvetti-type correlation functional. J Chem Phys 1999;110:10664–78https://doi.org/10.1063/1.479012.

[50] Yanai T, Tew DP, Handy NC. A new hybrid exchange–correlation functional using the Coulomb-attenuating method (CAM-B3LYP). Chem Phys Lett 2004;393:51–7https://doi.org/10.1016/j.cplett.2004.06.011.

[51] Peach MJG, Benfield P, Helgaker T, Tozer DJ. Excitation energies in density functional theory: an evaluation and a diagnostic test. J Chem Phys 2008;128:044118https://doi.org/10.1063/1.2831900.

[52] Zhang XF, Zhang I, Liu L. Photophysics of halogenated fluoresceins: involvement of both intramolecular electron transfer and heavy atom effect in the deactivation of excited states. Photochem Photobiol 2010;86:492–8https://doi.org/10.1111/j.1751-1097.2010.00706.x.

[53] Valeur B, Berberan-Santos MN. Molecular fluorescence: principles and applications. second ed. Weinheim, Germany: Wiley-VCH; 2012https://doi.org/10.1002/9783527650002.

[54] Alvarez-Pez JM, Ballesteros L, Talavera E, Yguerabide J. Fluorescein excited-state proton exchange reactions: nanosecond emission kinetics and correlation with steady-state fluorescence intensity. J Phys Chem A 2001;105:6320–32https://doi.

org/10.1021/jp010372+.
[55] Orte A, Talavera EM, Maçanita AL, Orte JC, Alvarez-Pez JM. Three-state 2',7'-difluorofluorescein excited-state proton transfer reactions in moderately acidic and very acidic media. J Phys Chem A 2005;109:8705–18https://doi.org/10.1021/jp051264g.
[56] Houari Y, Jacquemin D, Laurent AD. Methodological keys for accurate pK_a^* simulations. Phys Chem Chem Phys 2013;15:11875–82https://doi.org/10.1039/c3cp50791b.
[57] Tuna D, Spörkel L, Barbatti M, Thiel W. Nonadiabatic dynamics simulations of photoexcited urocanic acid. Chem Phys 2018;515:521–34https://doi.org/10.1016/j.chemphys.2018.09.036.
[58] Pijeau S, Foster D, Hohenstein EG. Effect of nonplanarity on excited-state proton transfer and internal conversion in salicylideneaniline. J Phys Chem A 2018;122:5555–62https://doi.org/10.1021/acs.jpca.8b02426.